Dioxygen Binding to Deoxyhemocyanin: Electronic Structure and Mechanism of the Spin-Forbidden Two-Electron Reduction of O_2

Markus Metz and Edward I. Solomon*

Contribution from the Department of Chemistry, Stanford University, 333 Campus Drive, Stanford, California 94305

Received December 4, 2000. Revised Manuscript Received March 15, 2001

Abstract: Spectroscopically calibrated DFT is used to investigate the reaction coordinate of O_2 binding to Hemocyanin (Hc). A reaction path is calculated in which O_2 approaches the binuclear copper site with increasing metal−ligand overlap, which switches the coordination mode from end-on η^1-η^1, to μ-η^1:η^2, then to butterfly, and finally to the planar [$Cu_2(\mu$-η^2:η^2O_2)] structure. Analysis of the electronic structures during O_2 binding reveals that simultaneous two-electron transfer (ET) takes place. At early stages of O_2 binding the energy difference between the triplet and the singlet state is reduced by charge transfer (CT), which delocalizes the unpaired electrons and thus lowers the exchange stabilization onto the separated copper centers. The electron spins on the copper(II) ions are initially ferromagnetically coupled due to close to orthogonal magnetic orbital pathways through the dioxygen bridging ligand, and a change in the structure of the Cu_2O_2 core turns on the superexchange coupling between the coppers. This favors the singlet state over the triplet state enabling intersystem crossing. Comparison with mononuclear model complexes indicates that the protein matrix holds the two copper(I) centers in close proximity, which enthalpically and entropically favors O_2 binding due to destabilization of the reduced binuclear site. This also allows regulation of the enthalpy by the change of the Cu−Cu distance in deoxyHc, which provides an explanation for the O_2 binding cooperativity in Hc. These results are compared to our earlier studies of Hemerythrin (Hr) and a common theme emerges where the spin forbiddeness of O_2 binding is overcome through delocalization of unpaired electrons onto the metal centers and the superexchange coupling of the metal centers via a ligand bridge.

1. Introduction

Respiratory proteins play a fundamental role for aerobic organisms. Three classes of oxygen carrier proteins have evolved: Hemoglobins (Hb),[1] Hemerythrins (Hr),[2] and Hemocyanins (Hc).[3−5] Hc are multisubunit proteins and are mainly found in mollusks and arthropods. Although their quaternary structures are very different the active sites of both proteins consist of a binuclear copper center which reversibly binds molecular oxygen.[6] The deoxy site has two cuprous ions, while in oxyhemocyanin (oxyHc) the two copper centers are oxidized and O_2 is reduced by two electrons to O_2^{2-}. In Chart 1 the structures of the binuclear copper site of oxygenated and deoxygenated arthropod Hc (deoxyHc) are displayed.[7−11] In oxyHc the peroxide is bound in an unusual side-on μ-η^2:η^2 bridged coordination mode. Both copper(II) ions have a local square pyramidal coordination geometry with two histidine ligands at 2.0 Å in the equatorial plane. The other two histidines bind in trans-axial positions to the copper(II) centers with a long distance of ∼2.4 Å. The copper(I) centers in deoxyHc have a distorted trigonal planar geometry with three normal Cu−N(His) bonds. There are two crystal structures of deoxyHc which mostly differ in their Cu−Cu distance and the pyramidal distortion from trigonal planar stereochemistry which increases with decreasing Cu−Cu distance. These crystal structures have been used to explain the experimentally observed cooperativity of O_2 binding by Hc which enables efficient O_2 uptake, delivery, and regulation.[9] The deoxyHc structure with the 4.6 Å Cu−Cu distance is thought to be in the tense (T) state while the structure with the shorter 3.5 Å Cu−Cu bond is believed to be relaxed (R-

Chart 1. Reversible O_2 Binding to Hc

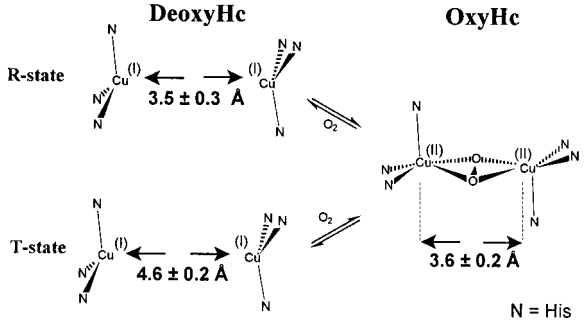

* Author to whom correspondence should be addressed.

(1) Niederhoffer, E. C.; Timmons, J. H.; Martell, A. E. *Chem. Rev.* **1984**, *84*, 137−203.
(2) Stenkamp, R. E. *Chem. Rev.* **1994**, *94*, 715−726.
(3) Solomon, E. I.; Baldwin, M. J.; Lowery, M. D. *Chem. Rev.* **1992**, *92*, 521−542.
(4) Solomon, E. I.; Tuczek, F.; Root, D. E.; Brown, C. A. *Chem. Rev.* **1994**, *94*, 827−856.
(5) Solomon, E. I.; Sundaram, U. M.; Machonkin, T. E. *Chem. Rev.* **1996**, *96*, 2563−2605.
(6) Van Holde, K. E.; van Bruggen, E. F. In *Subunits in Biological Systems*; Timasheff, S. N., Fasman, G. D., Eds.; Marcel Decker: New York, 1971; pp 1−53.
(7) Hazes, B. A.; Magnus, K. A.; Bonaventura, C.; Bonaventura, J.; Dauter, Z.; Kalk, K. H.; Hol, W. G. J. *Protein Sci.* **1993**, *2*, 597−619.
(8) Magnus, K. A.; Ton-That; Carpenter, J. E. In *Bioinorganic Chemistry of Copper*; Karlin, K. D., Tyeklar, Z., Eds.; Chapman & Hall: New York, 1993; pp 143−150.
(9) Magnus, K. A.; Hazes, B.; Ton-That, H.; Bonaventura, C.; Bonaventura, J.; Hol, W. G. J. *Proteins*: *Struct., Funct., Genet.* **1994**, *19*, 302−309.
(10) Magnus, K. A.; Ton-That, H.; Carpenter, J. E. *Chem. Rev.* **1994**, *94*, 727−735.
(11) Volbeda, A.; Hol, W. G. J. *J. Mol. Biol.* **1989**, *209*, 249−279.

10.1021/ja004166b CCC: $20.00
Published on Web 05/08/2001

state). The Cu−Cu distance of oxyHc is 3.6 Å. In this model, O_2 binding of the protein initially in the T-state would decrease the Cu−Cu distance by 1 Å, which could greatly affect the tertiary and quaternary structure and in turn reduce the Cu−Cu distance of other deoxygenated binuclear copper units and increase their O_2 affinity.

Synthetic modeling approaches have greatly increased our understanding of how O_2 interacts with the reduced binuclear copper sites.[12,13] The same $[Cu_2(\mu\text{-}\eta^2\text{:}\eta^2O_2)]^{2+}$ core has now been spectroscopically observed and crystallographically verified in a number of different tridentate N-ligand systems (derivatives of tris(pyrazolyl)hydridoborate,[14] 1,4,7-triazacyclononane,[13] bis-(2-pyridylethyl)amine linked by a *m*-xylylen spacer or by an aliphatic carbon chain[13]) which model the histidine local environment of the protein matrix. Also, mechanistic investigations have been performed which describe O_2 binding by biomimetic model complexes as enthalpically favorable as in the case of the Hc proteins. However, for the model complexes entropic terms are more unfavorable and reduce the stability of the peroxide complex.[13]

The unusual structural feature of the side-on bound peroxide coordination mode leads to unique spectral features.[3−5,15−17] The most obvious is the lack of an EPR signal that derives from antiferromagnetic coupling of the Cu(II) centers through the bridging peroxide ligand. Experimentally a lower limit for the coupling constant $-2J$ of >600 cm^{-1} was determined by SQUID magnetic susceptibility measurements. The absorption spectrum of the oxy site exhibits a very intense transition at 350 nm ($\epsilon \sim 20000$ M^{-1} cm^{-1}) and a weak feature at 550 nm ($\epsilon \sim 1000$ M^{-1} cm^{-1}) which are assigned as $O_2^{2-} \rightarrow$ Cu charge transfer (CT) transitions. The doubly degenerate π^* HOMOs of the peroxide are split in energy upon interaction with the binuclear copper site. The absorption band at higher energy is assigned as the $\pi^*_\sigma \rightarrow$ Cu(II) and the lower energy as the $\pi^*_v \rightarrow$ Cu(II) CT transition where π^*_σ is the peroxide orbital in the Cu_2O_2 plane (σ bonding to the Cu(II) centers) and the π^*_v is orthogonal (vertical) to the plane. The resonance Raman spectrum exhibits an extremely low O−O stretch vibration at 750 cm^{-1}, which indicates a very weak O−O bond and is explained by back-bonding from the copper centers into the σ^* LUMO of the peroxide. For deoxyHc, which has closed shell d^{10} Cu(I) centers, very few spectroscopic investigations[18−20] and no electronic structure description exists.[5]

Computational chemistry has provided fundamental insights into the electronic structure and reactivity of a variety of metalloproteins.[21,22] The $[Cu_2(\mu\text{-}\eta^2\text{:}\eta^2O_2)]^{2+}$ core has stimulated a number of theoretical investigations to understand its electronic structure, its spectroscopic properties,[16,17,23−32] the core isomerization to a bis-μ-oxo isomer $[Cu_2(\mu\text{-}O)_2]^{2+}$,[33−35] and its reaction in oxygenation of aromatic compounds.[36−39] For these studies, model systems with different numbers of nitrogen ligands $[\{(N)_nCu\}_2(\mu\text{-}\eta^2\text{:}\eta^2O_2)]^{2+}$ (N = NH_3, $n = 0, 1, 2, 3$; N = imidazole, $n = 3$) and computational methods using different levels of theory (EHT, INDO/S, SCF-Xα, HF, CASSCF, B3LYP, CASPT2) have been used.

In this study, the mechanism of reversible dioxygen binding to Hc is explored by utilizing DFT. First these density functional calculations are experimentally calibrated to past experimental, structural, and spectroscopic data on oxyHc. These calculations are extended to describe the electronic structure of deoxyHc and compared to Cu(I) K-edge data. A correlation of the electronic structure of deoxy to oxyHc provides the change in electronic structure on O_2 binding. These studies are then used to investigate the reaction coordinate of O_2 binding. One study of the process has appeared,[24] but it has not addressed the topics of charge transfer (CT) and intersystem crossing (ISC) investigated here. In the present study, the question as to whether there is a simultaneous or sequential two-electron transfer is considered and the mechanism of singlet−triplet intersystem crossing (S−T ISC) is evaluated. This is of crucial importance as O_2 binding is formally a spin-forbidden process (deoxyHc, singlet, O_2, triplet; oxyHc, singlet). These studies are then extended to the active site in the protein and effects considered which influence O_2 binding energetics and cooperativity. The results obtained for Hc are compared with the mechanism derived for O_2 binding to Hr,[40] and interesting common features emerge concerning the use of a bridged binuclear metal site to overcome the spin forbiddeness of this reaction.

2. Computational Details

All calculations were performed with the program package Gaussian 98[41] using the hybrid functional B3LYP[42,43] and the basis set Lanl2dz.[44−47] Because the two Cu(II) ions in oxyHc are antiferromagnetically coupled, the configuration wave function has multideterminantal character.[15] The broken-symmetry approach takes these nondynamic correlation effects

(12) Blackman, A. G.; Tolman, W. B. *Struct. Bonding* (*Berlin*) **2000**, *97*, 179−211.
(13) Karlin, K. D.; Tolman, W. B.; Kaderli, S.; Zuberbuhler, A. D. *J. Mol. Catal. A: Chemical* **1997**, *117*, 215−222.
(14) Kitajima, N.; Fujisawa, K.; Fujimoto, C.; Mor-oka, Y.; Hashimoto, S.; Kitagawa, T.; Tatsumi, K.; Nakamura, A. *J. Am. Chem. Soc.* **1992**, *114*, 1277−1291.
(15) Tuczek, F.; Solomon, E. I. *J. Am. Chem. Soc.* **1994**, *116*, 6916−6924.
(16) Ross, P. K.; Solomon, E. I. *J. Am. Chem. Soc.* **1991**, *113*, 3246−3259.
(17) Ross, P. K.; Solomon, E. I. *J. Am. Chem. Soc.* **1990**, *112*, 5871−5872.
(18) Woolery, G. L.; Powers, L.; Winkler, M.; Solomon, E. I.; Spiro, T. G. *J. Am. Chem. Soc.* **1984**, *106*, 86−92.
(19) Brown, J. M.; Powers, L.; Kincaid, B.; Larrabee; Spiro, T. G. *J. Am. Chem. Soc.* **1980**, *102*, 4210−4216.
(20) Co, M. S.; Hodgson, K. O. *J. Am. Chem. Soc.* **1981**, *103*, 3200−3201.
(21) Siegbahn, P. E. M.; Blomberg, M. R. A. *Chem. Rev.* **2000**, *100*, 421−437.
(22) Siegbahn, P. E. M.; Blomberg, M. R. A. *Annu. Rev. Phys. Chem.* **1999**, *50*, 221−249.
(23) Bernardi, F.; Bottoni, A.; Casadio, R.; Fariselli, P.; Rigo, A. *Int. J. Quantum Chem.* **1996**, *58*, 109−119.
(24) Bernardi, F.; Bottoni, A.; Casadio, R.; Fariselli, P.; Rigo, A. *Inorg. Chem.* **1996**, *35*, 5207−5212.
(25) Berces, A. *Inorg. Chem.* **1997**, *36*, 4831−4837.
(26) Berces, A. *Int. J. Quantum Chem.* **1997**, *65*, 1077−1086.
(27) Maddaluno, J.; Giessner-Prettre, C. *Inorg. Chem.* **1991**, *30*, 3439−3445.
(28) Eisenstein, O.; Getlicherman, H.; Giessner-Prettre; Maddaluno, J. *Inorg. Chem.* **1997**, *36*, 3455−3460.
(29) Getlicherman, H.; Giessner-Prettre, C.; Maddaluno, J. *J. Phys. Chem.* **1996**, *100*, 6819−6824.
(30) Liu, X.-Y.; Palacios, A. A.; Novoa, J. J.; Alvarez, S. *Inorg. Chem.* **1998**, *37*, 1202−1212.
(31) Estiu, G. L.; Zerner, M. C. *J. Am. Chem. Soc.* **1999**, *121*, 1893−1901.
(32) Erasmus, C.; Haase, W. *Inorg. Chim. Acta* **1994**, *221*, 141−146.
(33) Flock, M.; Pierloot, K. *J. Phys. Chem. A* **1999**, *103*, 95−102.
(34) Cramer, C. J.; Smith, B. A.; Tolman, W. B. *J. Am. Chem. Soc.* **1996**, *118*, 11283−11287.
(35) Henson, M. J.; Mukherjee, P.; Root, D. E.; Stack, T. D. P.; Solomon, E. I. *J. Am. Chem. Soc.* **1999**, *121*, 10332−10345.
(36) Pidcock, E.; Obias, H. V.; Zhang, C. X.; Karlin, K. D.; Solomon, E. I. *J. Am. Chem. Soc.* **1998**, *120*, 7841−7847.
(37) Pidcock, E.; Obias, H. V.; Abe, M.; Liang, H. C.; Karlin, K. D.; Solomon, E. I. *J. Am. Chem. Soc.* **1999**, *121*, 1299−1308.
(38) Lind, T.; Siegbahn, P. E. M.; Crabtree, R. H. *J. Phys. Chem. B* **1999**, *103*, 1193−1202.
(39) Eisenstein, O.; Giessner-Prettre, C.; Maddaluno, J.; Stussi, D.; Weber, J. *Arch. Biochem. Biophys.* **1992**, *296*, 247−255.
(40) Brunold, T. C.; Solomon, E. I. *J. Am. Chem. Soc.* **1999**, *121*, 8288−8295.

into account within DFT and has been employed with considerable success in interpreting the magnetic and spectroscopic properties of molecules with such ground-state configuration wave functions.[48−50] However, calculations on the model system $[\{(H_3N)_3Cu\}_2(\mu\text{-}\eta^2\text{:}\eta^2O_2)]^{2+}$ show that the use of the hybrid functional B3LYP is crucial to obtain a localized solution for the singlet state wave function. All attempts with pure density functional methods (e.g. BP86) converged to the symmetrical, fully delocalized solution of the ground-state wave function. Because the localized broken-symmetry state does not correspond to a pure singlet ground state a scheme was applied that weights the singlet and triplet contributions according to the value of $\langle S^2\rangle$ to derive the energy of the pure singlet ground state. An approximate spin projection developed by Noodleman[48] to derive the energy of the pure singlet ground state from $E(0) = [(S_{max} + 1)E_{BS} - E(S_{max})]/S_{max}$ yields qualitatively the same results. However, the slope of the spin-projected singlet state around $R \sim 0.0$ Å is steeper. The triplet states represent pure spin states with $\langle S^2\rangle$ deviating from 2.00 by not more than 0.0123.

Although B3LYP/Lanl2dz calculations show that the copper-ligand bonding description of D_{4h} $[CuCl_4]^{2-}$ is too covalent, the Lanl2dz basis set was chosen in our studies to enable geometry optimizations on a reasonable time scale.[51] The replacement of the histidines by NH_3 ligands is justified by past studies.[16,17] Geometry optimizations for $[\{(H_3N)_3Cu\}_2(\mu\text{-}\eta^2\text{:}\eta^2O_2)]^{2+}$ in the method calibration were performed in C_{2h} symmetry, which is also the symmetry reflected by the copper ligands in the crystal structure of oxyHc and the biomimetic model complexes. Partial geometry optimizations were performed in C_1 symmetry for $[(H_3N)_3CuCu(NH_3)_3]^{2+}$. The Time-Dependent Density Functional Theory formalism (TD-DFT)[52,53] was used to calculate the absorption spectrum of the model system $[\{(H_3N)_3Cu\}_2(\mu\text{-}\eta^2\text{:}\eta^2O_2)]^{2+}$.

For O_2 release, a reaction coordinate R is chosen that represents the distance between the center of mass of the O_2 and the $[(H_3N)_3CuCu(NH_3)_3]^{2+}$ moieties (Figure 1). For different values of R, partial geometry optimizations are performed with C_1 symmetry (a similar approach was used in another study[24]). In addition to R, the geometries of the NH_3 ligands (N−H bond lengths, H−N−H angles) were kept fixed at values optimized for the side-on bound peroxide complex within the broken-symmetry state. Calculations have also shown that the torsion angles N−Cu−Cu−N have to be fixed. This is in line with X-ray structures of the protein which show the imidazole ligands as part of a hydrogen-bonded network.[11] A perfectly staggered orientation is assumed. Two sets of geometry optimizations have been performed. In the first set of calculations the copper−copper distance was optimized. In the second set of calculations this value was restricted to 3.5 Å (Supporting Information, S5). This approach was necessary because the repulsive interaction between the two copper(I) units leads to dissociation at $R > 1.0$ Å. On the basis of the results of oxyHc in the method calibration section, geometry optimizations were performed in the closed shell singlet state. Then single point calculations for the triplet and broken-symmetry state were performed on these optimized structures. PCM calculations[54,55] have been performed with dielectric constants of $\epsilon = 4.0$ to simulate the protein environment and $\epsilon = 8.93$ for CH_2Cl_2. Thermodynamic data were derived from frequency calculations in the gas phase by including the solvent contribution on the electronic energy ($\Delta H(s) = \Delta H(g) - \Delta E_{elec,gas\ phase} + \Delta E_{elec,solv}$; $\Delta G(s) = \Delta G(g) - \Delta E_{elec,gas\ phase} + \Delta E_{elec,solv}$; s = solvents, g = gas phase). For some of the optimized geometries, frequency calculations have been performed which identify these as true minima. In some cases small imaginary frequencies have been calculated ($\nu > -40$ cm^{-1}) which still persist after reoptimization. The same was also observed by Flock at al.[33]

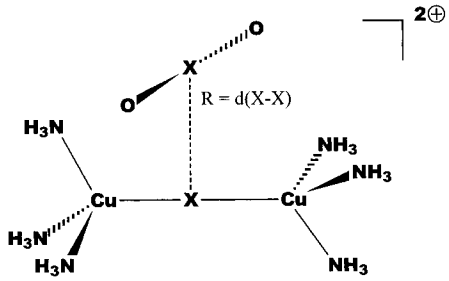

Figure 1. Model used for the reaction coordinate of O_2 binding to Hemocyanin. R is defined as the distance between the center of mass of the O_2 and the binuclear copper complex.

3. Results and Analysis

3.1. Method Calibration. In this section the agreement between spectroscopic data and results of calculations on the B3LYP/Lanl2dz level of oxyHc and deoxyHc will be evaluated. These insights will then be used for geometry optimizations of the O_2 reaction path.

3.1.1. Oxyhemocyanin. (a) Geometry Optimizations. In a first step, the geometry of $[\{(H_3N)_3Cu\}_2(\mu\text{-}\eta^2\text{:}\eta^2O_2)]^{2+}$ is optimized for different electronic states. In Table 1 important geometrical parameters obtained from B3LYP geometry optimizations (A) are listed together with experimentally determined structural parameters for the oxyhemocyanin active site of *L. polyphemus*[18,19,56] and for the biomimetic model compound $[\{HB(3,5\text{-}^iPr_2pz)_3Cu\}_2(\mu\text{-}\eta^2\text{:}\eta^2\ O_2)]$[14] (B). Given the limited size of the calculated model system and the uncertainties in the experimentally determined geometries of the protein crystal structures, the agreement is reasonable. The results are comparable to other computational studies performed at different levels of theory. A detailed discussion of the results of different computational studies is given by Flock et al.[33] Note that the structural differences as a function of the electronic state are comparable to the differences between the calculated and the experimentally determined geometries. This is important for further geometry optimizations.

(b) Spectroscopy. To evaluate the electronic structure description of the $[Cu_2(\mu\text{-}\eta^2\text{:}\eta^2O_2)]$ core, spectroscopic data are compared with calculations on the B3LYP/Lanl2dz level.

(41) Frisch, M. J.; Trucks, G. W.; Schlegel, H. B.; Scuseria, G. E.; Robb, M. A.; Cheeseman, J. R.; Zakrzewski, V. G.; Montgomery, J. A.; Strattmann, R. E.; Burant, J. C.; Dapprich, S.; Millam, J. M.; Daniels, A. D.; Kudin, K. N.; Strain, M. C.; Farkas, O.; Tomasi, J.; Barone, V.; Cossi, M.; Cammi, R.; Mennucci, B.; Pomelli, C.; Adamo, C.; Clifford, S.; Ochterski, J.; Petersson, G. A.; Ayala, P. Y.; Cui, Q.; Morokuma, K.; Malick, D. K.; Rabuck, A. D.; Raghavachari, K.; Foresman, J. B.; Cioslowski, J.; Ortiz, J. V.; Stefanov, B. B.; Liu, G.; Liashenko, A.; Piskorz, P.; Komaromi, I.; Gomperts, R.; Martin, R. L.; Fox, D. J.; Keith, T.; Al-Laham, M. A.; Peng, C. Y.; Nanayakkara, A.; Gonzalez, C.; Challacombe, M.; Gill, P. M. W.; Johnson, B. G.; Chen, W.; Wong, M. W.; Andres, J. L.; Head-Gordon, M.; Replogle, E. S.; Pople, J. A.; *Gaussian 98*, Revision A.7; Gaussian Inc.: Pittsburgh, PA., 1998.

(42) Becke, A. D. *J. Chem. Phys.* **1993**, *98*, 5648−5652.

(43) Stevens, P.; Devlin, F. J.; Chablowski, C. F.; Frisch, M. J. *J. Phys. Chem.* **1994**, *98*, 11623−11627.

(44) Dunning, T. H. J.; Hay, P. J. In *Modern Theoretical Chemistry*; Schaefer, H. F., III, Ed.; Plenum: New York, 1976; Vol. 3, pp 1−27.

(45) Hay, P. J.; Wadt, W. R. *J. Chem. Phys.* **1985**, *82*, 270−283.

(46) Wadt, W. R.; Hay, P. J. *J. Chem. Phys.* **1985**, *82*, 284−298.

(47) Hay, P. J.; Wadt, W. R. *J. Chem. Phys.* **1985**, *82*, 299−310.

(48) Li, J.; Noodleman, L.; Case, D. A. In *Inorganic Electronic Structure and Spectroscopy*; Solomon, E. I., Lever, A. B. P., Eds.; John Wiley & Sons: New York, 1999; Vol. I, pp 661−724.

(49) Lovell, T.; McGrady, J. E.; Stranger, R.; Macgregor, S. A. *Inorg. Chem.* **1996**, *35*, 3079−3080.

(50) McGrady, J. E.; Stranger, R.; Lovell, T. *J. Phys. Chem. A* **1997**, *101*, 6265−6272.

(51) Szilagyi, R. K.; Metz, M.; Solomon, E. I. Manuscript in preparation.

(52) Stratmann, R. E.; Scuseria, G. E.; Frisch, M. J. *J. Chem. Phys.* **1998**, *109*, 8218−8224.

(53) Casida, M. E. In *Recent Advances in Computational Chemistry*; Chong, D. P., Ed.; World Scientific: New York, 1995; Vol. 1, pp 155−192.

(54) Barone, V.; Cossi, M.; Tomasi, J. *J. Chem. Phys.* **1997**, *107*, 3210−3221.

(55) Miertus, S.; Scrocco, E.; Tomasi, J. *Chem. Phys.* **1981**, *55*, 117−129.

(56) Co, M. S.; Hodgson, K. O.; Eccles, T. K.; Lontie, R. *J. Am. Chem. Soc.* **1981**, *103*, 986−988.

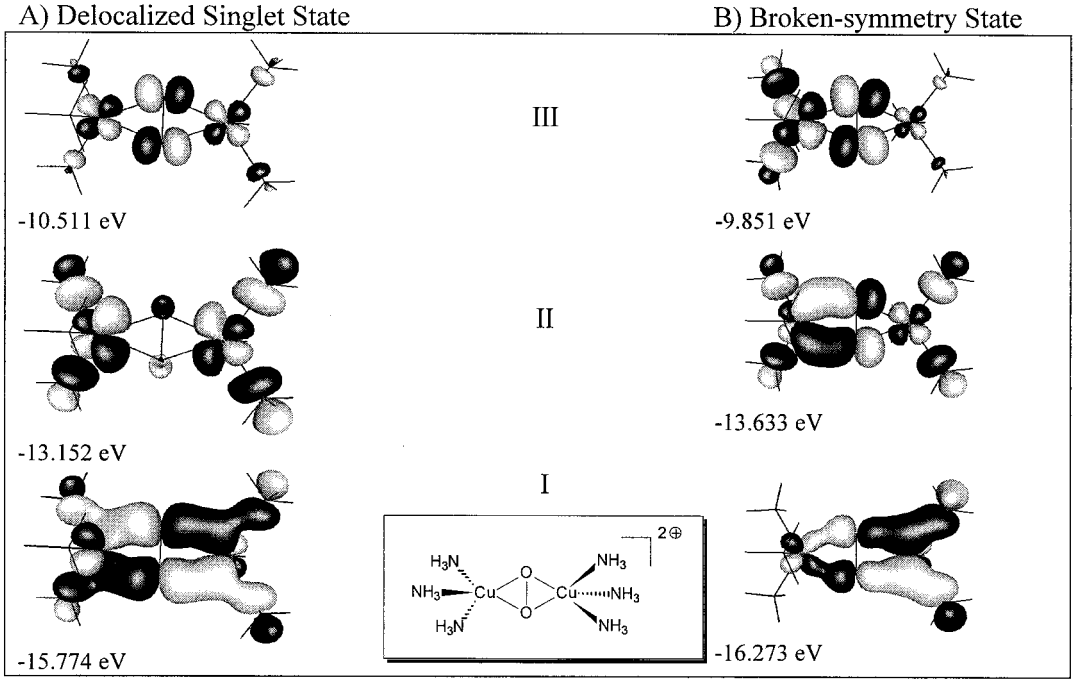

Figure 2. Molecular orbitals of the broken-symmetry and singlet state of the model $[\{(H_3N)_3Cu\}_2(\mu\text{-}\eta^2\text{:}\eta^2O_2)]^{2+}$ describing the Cu−O interaction. (IIIA,B, LUMO; IIA, HOMO; IIB, second highest occupied MO).

One characteristic feature of the $[Cu_2(\mu\text{-}\eta^2\text{:}\eta^2\ O_2)]$ core is the antiferromagnetic coupling between the two Cu(II) ions. Experimentally a lower limit of $>600\ cm^{-1}$ was determined for the exchange coupling constant $-2J$ by SQUID magnetic susceptibility measurements.[57,58] Therefore these calculations were used to determine the sign and magnitude of $-2J$. In the limit of two weakly interacting copper dimers, where the magnetic orbitals are localized on each metal (vide infra, Figure 2, right column), the calculated value of the ground-state singlet−triplet splitting, $-2J$ ($H = -2JS_1{*}S_2$), is twice the energy difference between the triplet and broken-symmetry state.[48] Although our calculated value of 7550 cm^{-1} is at the upper limit of previous calculated values (Table 2),[15−17,23−29,31−34,38,39] this large calculated antiferromagnetism is consistent with the observed diamagnetism.

The very low O−O stretch vibration of 750 cm^{-1} is another important spectroscopic property of the $[Cu_2(\mu\text{-}\eta^2\text{:}\eta^2O_2)]$ core.[59,60] The calculated B3LYP/Lanl2dz result of 845 cm^{-1} lies between the experimental value and the only other calculated value reported in the literature (Table 3).[33]

An important spectroscopic probe for the peroxide−Cu_2(II) interaction is the absorption spectrum.[3,14,15] Calculations so far have greatly overestimated the $\pi^*_\sigma \rightarrow$ Cu(II) CT energy as they do not properly take into account the multideterminantal character of the excited state. However, the TD-DFT describes excitations with significant two-electron character [61] and was applied successfully for transition metal compounds.[62,63] Therefore the absorption spectrum of the model $[\{(H_3N)_3Cu\}_2(\mu\text{-}\eta^2\text{:}\eta^2\ O_2)]^{2+}$ was calculated with the TD-DFT formalism. The results are given in Table 4. The main features of the experimental spectrum are reproduced. An intense $\pi^*_\sigma \rightarrow$ Cu(II) CT at 28000 cm^{-1}, a weak absorption band at 16000 cm^{-1} having $\pi^*_\sigma \rightarrow$ Cu(II), $\pi^*_v \rightarrow$ Cu(II), and d → d character, and d → d transitions at 14400 cm^{-1} are in good agreement with experiment. However, the calculation has an additional dominantly $\pi^*_v \rightarrow$ Cu(II) CT transition at very low energy.

(c) Electronic Structure. For the analysis of the electronic structure of the model system $[\{(H_3N)_3Cu\}_2(\mu\text{-}\eta^2\text{:}\eta^2\ O_2)]^{2+}$, selected molecular orbitals of the broken-symmetry state are compared with those of the fully delocalized singlet state (Figure 2). The major contribution to the strength of the copper−peroxide bonds is the σ bonding interaction between the positive linear combination of the Cu d_{xy} orbitals and the in-plane peroxide π^*_σ orbital (Figure 2: I, bonding; III, antibonding counterpart). This is in agreement with prior studies on the X_α-SW level.[16,17] The calculations also show a small contribution of the σ^*_{O-O} orbital to the Cu−O bonding (Figure 2, IIA) that is responsible for the low O−O stretching frequency. This is not obvious in the broken-symmetry calculation because of the very large π^*_σ contribution in the broken-symmetry wave function (Figure 2, IIB).

The comparison between calculated and experimentally determined data is reasonable but indicates an inverted bonding description in which the copper orbitals are energetically lower than the ligand orbitals. The inclusion of exact exchange into the B3LYP functional improves the bonding description relative to pure density functional GGA calculations. This localizes the singlet state. However, the analysis of the electronic structure of $[\{(H_3N)_3Cu\}_2(\mu\text{-}\eta^2\text{:}\eta^2\ O_2)]^{2+}$ (Figure 2) shows only a negligible contribution of the σ^*_{O-O} orbital in the copper oxygen bonding, which explains the difference in the calculated and experimentally determined O−O stretch vibration. In line with this is that the calculated $\pi^*_v \rightarrow$ Cu(II) CT is too low in energy at 6300 cm^{-1}. Destabilization of the copper orbitals relative to

(57) Solomon, E. I.; Dooley, D. M.; Wang, R. H.; Gray, H. B.; Cerdonio, M.; Mogno, F.; Romani, G. L. *J. Am. Chem. Soc.* **1976**, *98*, 1029−1031.
(58) Dooley, D. M.; Scott, R. A.; Ellinghaus, J.; Solomon, E. I.; Gray, H. B. *Proc. Natl. Acad. Sci. U.S.A.* **1978**, *75*, 3019−3022.
(59) Larrabee, J. A.; Spiro, T. G. *J. Am. Chem. Soc.* **1980**, *102*, 4217−4223.
(60) Freedman, T. B.; Loehr, J. S.; Loehr, T. M. *J. Am. Chem. Soc.* **1976**, *98*, 2809−2815.
(61) Hirata, S.; Head-Gordon, M. *Chem. Phys. Lett.* **1999**, *302*, 375−382.
(62) Rosa, A.; Baerends, E. J.; van Gisbergen, S. J. A.; van Lenthe, E.; Groeneveld, J. A.; Snijders, J. G. *J. Am. Chem. Soc.* **1999**, *121*, 10356−10365.
(63) van Gisbergen, S. J. A.; Groeneveld, J. A.; Rosa, A.; Snijders, J. G.; Baerends, E. J. *J. Phys. Chem. A* **1999**, *103*, 6835−6844.

Table 1. $Cu_2O_2N_6$ Core Bond Lengths [Å] of $[\{(H_3N)_3Cu\}_2(\mu\text{-}\eta^2\text{:}\eta^2O_2)]^{2+}$ and Protein Sites and a Biomimetic Model Complex

(A) $[\{(H_3N)_3Cu\}_2(\mu\text{-}\eta^2\text{:}\eta^2O_2)]^{2+}$

method/basis	state	d(Cu−Cu)	d(O−O)	d(Cu−O)	d(Cu−N_{ax})	d(Cu−N_{eq})
B3LYP/Lanl2dz	^1A_g	3.82	1.47	2.05	2.21	2.07
bs-B3LYP/Lanl2dz	^1A_g	3.78	1.52	2.04	2.21	2.07
B3LYP/Lanl2dz	^3B_u	3.82	1.56	2.06	2.20	2.06

(B) Protein Sites and a Biomimetic Model Complex

method	d(Cu−Cu)	d(O−O)	d(Cu−O)	d(Cu−N_{ax})	d(Cu−N_{eq})
X-ray (model complex)	3.560	1.412	1.915	2.258	1.997
X-ray (Limulus II)	3.6 ± 0.2	1.4	2.0	2.4	2.1
EXAFS (Limulus)	3.62		1.86		1.98

Table 2. Singlet−Triplet Splitting, $\Delta E_{t-s} = -2J$ (cm^{-1}), of the Model System $[\{(H_3N)_3Cu\}_2(\mu\text{-}\eta^2\text{:}\eta^2O_2)]^{2+}$

method	$-2J$
experiment	≥600
bs-B3LYP/Lanl2dz	7550
lit. calculation	2500−6800

Table 3. Experimental and Calculated O−O Stretch Vibration [cm^{-1}] of the Model System $[\{(H_3N)_3Cu\}_2(\mu\text{-}\eta^2\text{:}\eta^2\ O_2)]^{2+}$ in the $M_s = 0$ State

	ν(O−O)
experiment	740−750
bs-B3LYP/Lanl2dz	845
lit. calculation	986

Table 4. Experimental Absorption Spectrum of OxyHc and Calculated Spectrum of $[\{(H_3N)_3Cu\}_2(\mu\text{-}\eta^2\text{:}\eta^2\ O_2)]^{2+}$ in the $M_s = 0$ State (TD-B3LYP/Lanl2dz)

assignments	ΔE_{calc} [cm^{-1}]	ΔE_{exp} [cm^{-1}]
$\pi^*_v \rightarrow$ Cu(II)	6310 (0.001)	
d → Cu(II)x	14340 (0.001)	14800 (vw)
d,π^*_v,π^*_σ → Cu(II)	15968 (0.024)	18600 (w)
$\pi^*_\sigma \rightarrow$ Cu(II)	28047 (0.397)	28600 (s)

the ligand orbitals would yield a better agreement between experiment and calculations. This would increase the π^*_v character in the 16000 cm^{-1} band, and the σ^*_{O-O} orbital would have greater participation in back-bonding. Overall, these calculations show a qualitatively proper description of the electronic structure of the $[Cu_2(\mu\text{-}\eta^2\text{:}\eta^2O_2)]$ core which should give valuable insights for the O_2 reaction pathway.

3.1.2. Deoxyhemocyanin. To analyze the electronic structure of the reduced site, calculations of the model complex $[(H_3N)_3CuCu(NH_3)_3]^{2+}$ are compared with its mononuclear fragment $[Cu(NH_3)_3]^+$. The geometry optimization of the complex $[Cu(NH_3)_3]^+$ on the B3LYP/Lanl2dz level yields a trigonal planar structure typical for d^{10}-ML_3 units.[64] The electronic structure shows two nonbonding d_{xz} and d_{yz} MOs. Antibonding ligand interactions destabilize the d_{z^2} MO and to a greater extend the degenerate d_{xy} and $d_{x^2-y^2}$ MOs, which form the HOMO pair (Figure 3).

On the basis of the d^{10} electronic structure of the mononuclear fragment no bonding interaction between the two coppers is expected in the binuclear complex $[(H_3N)_3CuCu(NH_3)_3]^{2+}$. This is supported by geometry optimizations. All attempts fail to prevent the complex from dissociating into two $[Cu(NH_3)_3]^+$ fragments. Therefore restricted geometry optimizations in which the copper−copper distance is fixed to 3.5 and 4.6 Å were performed. These are the structures of the tense and relaxed

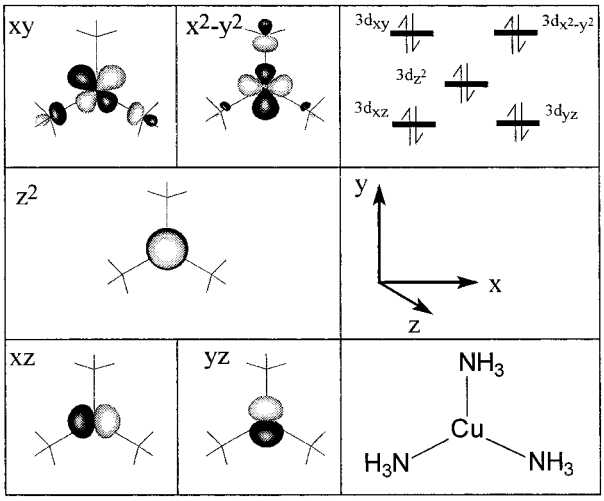

Figure 3. Molecular orbitals of the mononuclear model complex $[(H_3N)_3Cu]^+$.

Table 5. Important Geometric Data of the Binuclear Copper(I) Active Site of the Model Complex (calculation) and the Proteins (experiment)

method	d(Cu−Cu) [Å]	d(Cu−N) [Å]	∠(Cu−N(N_3)) [deg][a]
$[(NH_3)_3CuCu(NH_3)_3]^{2+}$	3.5	2.1, 2.1, 2.1 2.1, 2.1, 2.1	17.5, −17.3
$[(NH_3)_3CuCu(NH_3)_3]^{2+}$	4.6	2.1, 2.1, 2.1 2.1, 2.1, 2.1	13.4, −13.4
X-ray (Panilurus)[b]	3.5 ± 0.3	2.7, 2.0, 2.0 2.7, 2.1, 2.0	49.4, −43.5
X-ray (Limulus II)	4.6 ± 0.2	2.1, 2.0, 1.9 2.2, 2.1, 1.9	15.9, −37.4

[a] Angular distortions of the Cu−N bond out of the N_3 plane. Only the largest distortion value is given. [b] Average of the values of the six molecules in the crystallographic asymmetric unit.

state of deoxyHc. The local coordination structure of the copper(I) units in the optimized geometries exhibits a distortion of the copper out of the plane formed by the three nitrogen atoms with a staggered ligand conformation as in crystal structures of the deoxyHc active sites (Chart 1, left). As Table 5 shows, this pyramidal distortion increases as the copper−copper distance decreases.[65]

The effect of this distortion is observed in Cu K-edge X-ray absorption spectra of deoxyHc. X-ray absorption data have been used with considerable success in defining the coordination number and geometry of Cu(I) sites in proteins and model complexes.[3−5,66] Comparison with a trigonal planar model compound yields a less intense $1s \rightarrow 4p_z$ transition shifted to higher energy (A vs D in Figure 4, left) that is in agreement

(64) Albright, T. A.; Burdett, J. K.; Whangbo, M.-H. *Orbital Interactions in Chemistry*; John Wiley & Sons: New York, 1985.

(65) See Figure 4 right for a schematic representation of the pyramidal distortion.

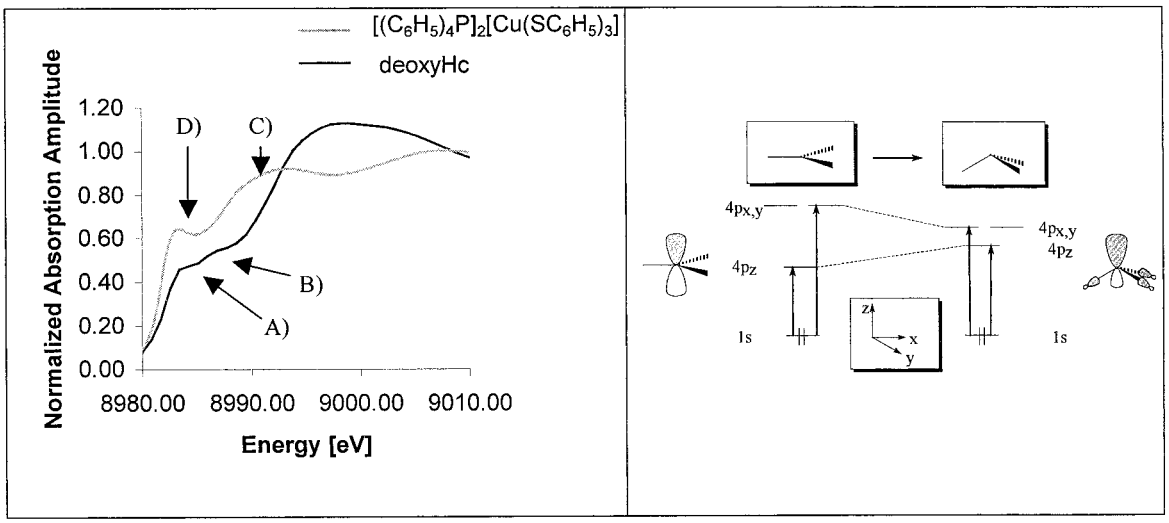

Figure 4. Left: Normalized Cu K-edge spectra of deoxyHc and a trigonal planar [CuS_3] model compound, adapted from reference[66]. Right: The ligand field splitting of the copper 4p orbitals and the 1s→4p transitions are shown. Assignment of deoxyHc is based on a mononuclear model complex since the electronic interaction between the two Cu(I) moieties is negligible.

with an increased Cu $4p_z$ ligand interaction upon pyramidal distortion (Figure 4, right).

The second peak of the pre-edge feature of deoxyHc is the $1s \rightarrow 4p_{x,y}$ transition (B in Figure 4, left). The $1s \rightarrow 4p_{x,y}$ transitions of the model compound are shifted to higher energy into the edge of the spectrum (C in Figure 4, left) consistent with an increase in the ligand field in the *xy* plane due to the trigonal planar structure.

The electronic structure of the model complex $[(H_3N)_3CuCu(NH_3)_3]^{2+}$ corresponds to two repelling $[Cu(NH_3)_3]^{+}$ fragments in which all 10 MOs with mainly Cu-d character are fully occupied. The trigonal pyramidal distortion in $[(H_3N)_3CuCu(NH_3)_3]^{2+}$ has only a minor effect on the MOs which resemble a combination of two isolated mononuclear units. The splitting of bonding and antibonding linear combinations of the $[Cu(NH_3)_3]^{+}$ FMO's with mainly d-character is smaller than 2.5 kcal/mol. Therefore, the energy difference of 52 (d(Cu−Cu) = 4.6 Å) and 58 kcal/mol (d(Cu−Cu) = 3.5 Å) between the $[(H_3N)_3CuCu(NH_3)_3]^{2+}$ and the isolated fragments is mainly of electrostatic origin. The inclusion of solvent effects to simulate the protein environment ($\epsilon = 4.0$) lowers these energy differences to 18 (d(Cu−Cu) = 4.6 Å) and 21 kcal/mol (d(Cu−Cu) = 3.5 Å). For the same distances the calculated electrostatic interactions between two positive point charges in the gas phase are +72 and +95 kcal/mol.

Comparison of the geometric and electronic structure of the model complexes for oxyHc and deoxyHc yields insight into the electronic structure changes on O_2 binding. The redox active orbitals of the reactants at large distance are the occupied plus linear combination of the d_{xy} orbitals of the $[Cu(NH_3)_3]^{+}$ fragments and the half-occupied π^* O_2 orbitals (left side of Figure 5). During O_2 coordination a major ligand reorientation changes the copper coordination geometry from distorted trigonal planar to square pyramidal. The change of the ligand field rotates and destabilizes the redox active copper orbitals favoring electron transfer (Figure 5). Charge contributions reveal that the LUMO of the side-on bound peroxide complex has more copper character indicating a redox process has occurred (vide infra: Figure 9; $R = 0.0$ Å) and both π^* O_2 orbitals are fully occupied. On the basis of the near degeneracy of the highest occupied orbitals of deoxyHc (Figure 3, linear combinations of d_{xy} and $d_{x^2-y^2}$), there is no preference for the side-on binding mode at larger copper−oxygen distances and other binding modes, e.g., an end-on η^1-η^1 coordination, become feasible.

3.2. O_2 Binding/Release. 3.2.1. Geometry Optimizations. Optimized geometries for the closed shell singlet state are shown in Figure 6. Starting from the peroxide-bridged binuclear copper complex the successive increase of R yields first a symmetric dissociation of the peroxide ligand into a butterfly structure. Then, at approximately $R = 0.6$ Å the coordination mode changes and the substrate interacts first in an μ-η^1:η^2 fashion with both coppers and then at larger distances ($R = 1.0$ Å) in an end-on η^1-η^1 coordination manner. The increasing Cu(I) character (vide supra) makes geometry optimizations more difficult for larger values of R without constraining the copper−copper distance.

Because of the large copper−copper distance of around 4.2 Å in the nonsymmetric coordination modes ($R = 0.7$ and 1.0 Å in Figure 6), these investigations can be viewed as the O_2 binding/release pathway for the T-state of Hc. Calculations have also been performed with the copper−copper distance kept fixed to 3.5 Å, modeling the situation for the protein in the R-state. These calculations could be extended to larger values of R (0.8 Å $\leq R \leq$ 3.0 Å) and yield the same basic results (Supporting Information, S5). However, because of the restricted copper−copper distance the end-on η^1-η^1 coordination mode occurs at larger values of R.

The approach used to evaluate the reaction coordinate of the O_2 binding/release (Figure 1) also allows for the possibility of formation of nonsymmetrically bound superoxo−copper species. As the copper−oxygen distances for $R = 0.6$ Å (Figure 6) indicate, during the oxygen release in the symmetric coordination mode the peroxide interacts slightly more strongly with one copper center. However, at larger values of R, the nonsymmetric μ-η^1:η^2 bridging mode preferrably forms over the η^2 superoxo geometry during the reaction. Similarly, a nonsymmetric end-on geometry is indicated during O_2 release in the relaxed state (Supporting Information, S5). At $R = 2.0$ Å the trans end-on coordination mode (similar to the geometry at $R = 1.0$ Å in Figure 6) exhibits different copper−oxygen bond lengths of 2.420 and 2.177 Å. However, at values of $R >$

(66) (a) Model complex: Kau, L.-S.; Spira-Solomon, D. J.; Penner-Hahn, J. E.; Hodgson, K. O.; Solomon, E. I. *J. Am. Chem. Soc.* **1987**, *109*, 6433−6442. (b) deoxyHc: Kau, L.-S.; Hodgson, K. O.; Solomon, E. I. Unpublished results.

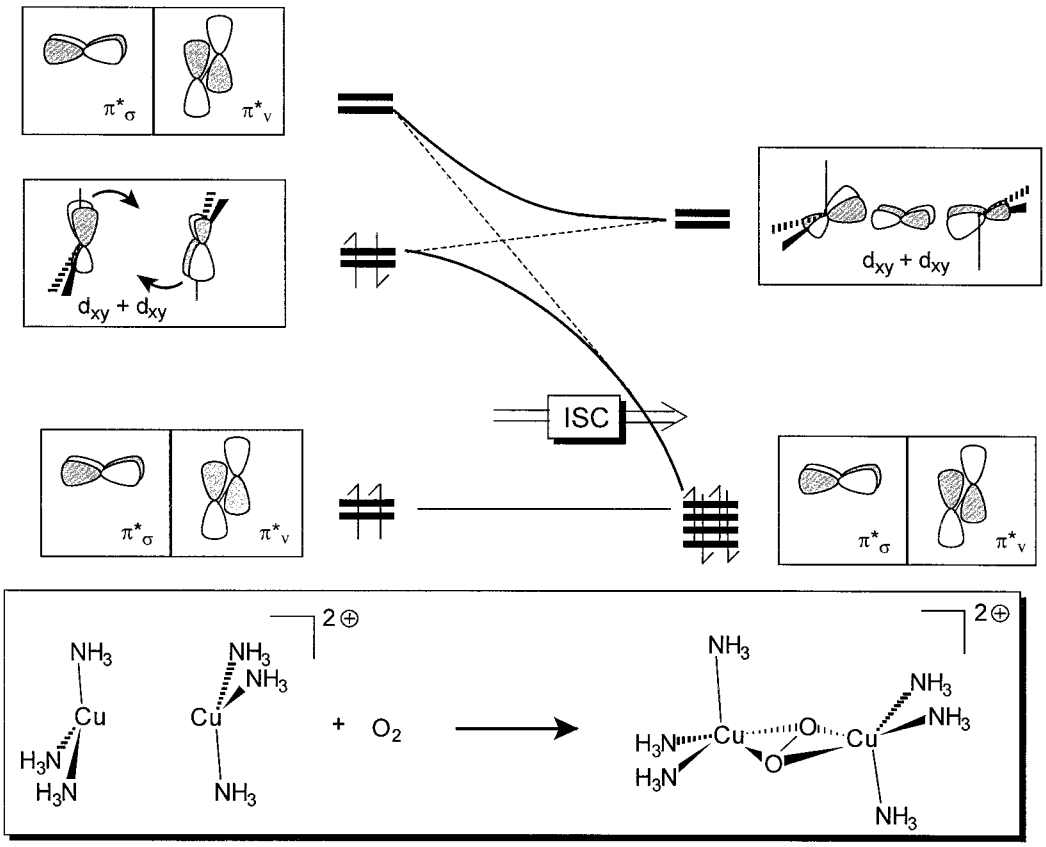

Figure 5. Orbital correlation diagram for the O_2 binding to $[(H_3N)_3CuCu(NH_3)_3]^{2+}$. For clarity the NH_3 ligands are indicated by lines.

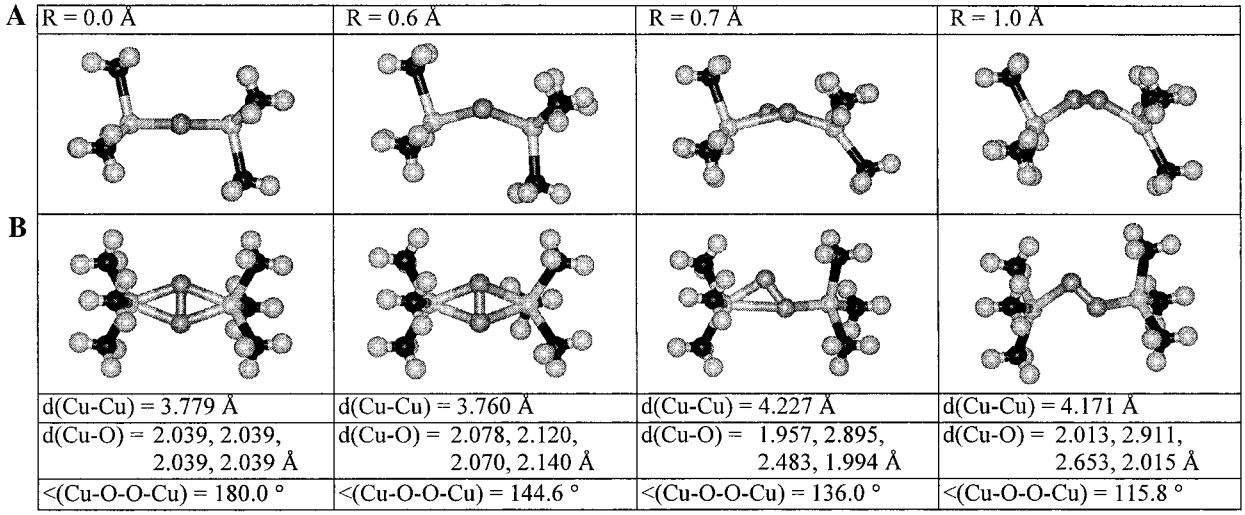

Figure 6. Optimized geometries for the interconversion of oxyHc and deoxyHc as a function of the reaction coordinate *R*: (A) view along the O−O bond in the $[Cu_2(\mu\text{-}\eta^2\text{:}\eta^2O_2)]$ complex and (B) molecules rotated around the copper−copper vector by 90°.

2.0 Å this asymmetry is no longer observed. Because the population analysis for $R \geq 2.0$ Å shows only a weak interaction between O_2 and the binuclear copper(I) site, no further attempts were made to obtain an end-on bound superoxo complex (Supporting Information, S7).

These results are consistent with the idea that the substrate approaches the binuclear copper(I) site driven by optimizing the metal−ligand overlap. At early stages of O_2 binding two competing pathways, mono- and binuclear O_2 binding modes, can exist. However, the closer the substrate approaches the binuclear copper site the greater the bridged binuclear binding mode is preferred. This is supported by the preference for a $\mu\text{-}\eta^1\text{:}\eta^2$ coordination mode over an η^2 superoxo geometry and by the energetically preferred two- versus one-electron reduction of O_2 (see below).

3.2.2. Charge Transfer (CT). The analysis of the electronic structures of these optimized geometries in their triplet and broken-symmetry configurations gives important insight into the nature of the redox process. In Figure 7 the partial charges (*Q*) of the copper and oxygen atoms during the symmetric (vide infra: Figure 8, $R = 0.0$ to 0.7 Å) and nonsymmetric O_2 release (vide infra: Figure 8, $R = 0.6-1.0$ Å) are presented. The changes of *Q* of both of the copper and oxygen atoms within our model for the T-state (Figure 6) are very similar during O_2 release.[67] The *Q* of the oxygen and copper atoms continuously evolve as expected. The copper ions are reduced as shown by

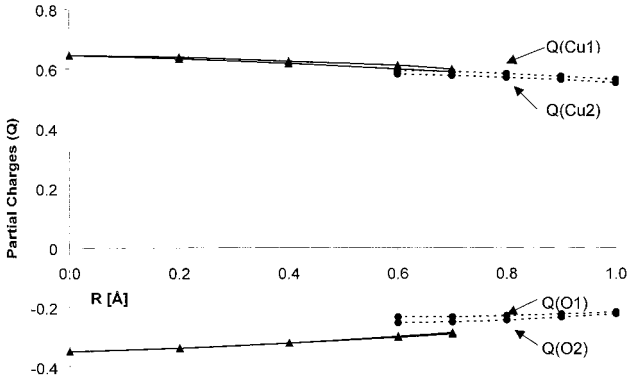

Figure 7. Change of partial charges of the copper and oxygen atoms during the O_2 release from oxyHc; results are from Mulliken population analysis along the pathway: singlet symmetric O_2 coordination ↔ triplet nonsymmetric O_2 coordination (Figure 6); solid lines for symmetric O_2 coordination; dashed lines for nonsymmetric coordination; (●) triplet state; (▲) singlet state. At each R two values of the copper and the oxygen atoms are presented for a given coordination mode.

the decrease of their Q. The oxidation of the oxygen atoms is indicated by a decrease of their negative Q. The Mulliken population analysis of the results of the second set of calculations in which the copper−copper distance is fixed to 3.5 Å confirms these trends and at $R = 3.0$ the substrate dioxygen has completely formed (Supporting Information, S7). *The similar changes of the Q of the two coppers and two oxygen atoms reveal that this is a simultaneous 2-electron-transfer process.*[68] The nonsymmetric O_2 coordination modes for $R \geq 0.6$ Å (Figure 6) have only a minor influence on the charge distribution on the atoms.

3.2.3. Singlet−Triplet Intersystem Crossing (S−T ISC). The energy surface in Figure 8 shows that at early stages of O_2 release the spin projected pure singlet state with a symmetric coordination of the peroxide is energetically preferred ($R < 0.6$ Å). With increasing R the energy difference to the triplet state decreases until at around $R = 0.6$ Å ISC takes place. During or after the ISC the O_2 coordination mode changes from μ-η^2:η^2 to μ-η^1:η^2 and the process follows the triplet state potential surface. The flat energy surface does not allow a correlation of the change of the O_2 coordination mode to the change in the electronic state.

The ISC results from the bending of the two Cu_2O planes in early stages of O_2 release (see torsion angles in Figure 6). In the planar μ-η^2:η^2 peroxide complex the singlet state is favored over the triplet state by a superexchange mechanism in which the π^*_σ peroxide orbital functions to couple the two copper atoms. In contrast, the π^*_v peroxide orbital has mainly nonbonding character and therefore its energy difference to the π^*_σ peroxide orbital is 0.95 eV. This energy difference is decreased by the bending of the two Cu_2O planes because of an additional interaction of the occupied π^*_v orbital on the peroxide ligand with the formally unoccupied copper-d orbitals (vide infra: Figure 9). In parallel the interaction between the π^*_σ and the copper-d orbitals is reduced. Thus, the π^* orbitals are closer in energy and are more easily rehybridized to form close to orthogonal orbitals, one directed to each copper. These are the magnetic orbitals, and their orthogonality during the butterfly distortion eliminates superexchange stabilization of the singlet state.

The reduction of the superexchange pathway is reflected by the decreased contribution of the second copper atom to the LUMO[69] upon the ring puckering of the $[Cu_2(\mu$-η^2:$\eta^2O_2)]$ core (Figure 9; butterfly distortion from $R = 0.0$ to 0.6 Å). In the extreme case of a 90° angle between the two CuO_2 planes the two copper ions would interact through orthogonal π^*_{O-O} orbitals, and the contribution of the second copper atom to the LUMO is zero (Figure 10A). Thus, *the ISC is favored by the increased orthogonality of the magnetic orbitals in the butterfly geometry*.

In the triplet state the butterfly distortion of the $[Cu_2(\mu$-η^2:$\eta^2O_2)]$ core enables CT out of orthogonal π^* O_2^{2-} orbitals which directly correlates with the $^3\Sigma_g^-$ ground state of O_2 where the increased exchange interaction further stabilizes the triplet state over the singlet state (Figure 10B).[70]

3.2.4. Energetics. Although the above investigations give important insights into ISC and CT, the energy surfaces shown in Figure 8 are in a vacuum and thus do not represent the actual energetic situation for the O_2 coordination/release of the binuclear copper site in the protein. The peroxide complex should be relatively independent of the protein environment as the $[(N)_3Cu]_2(\mu$-η^2:$\eta^2O_2)^{2+}$ unit is very similar to that in the crystal structures of the Hcs and to that in the biomimetic model complexes. Alternatively, the influence of the protein matrix on the binuclear copper(I) site is rather large. As indicated above, there is no bonding interaction between two Cu(I) units. Nevertheless, these copper ions are held in close proximity in the protein matrix. Therefore, to estimate the thermodynamics of O_2 binding in the protein, the geometries of the mono- and binuclear copper complexes were optimized and characterized as minima,[71] and their solvation energies were calculated. The results are shown in Figure 11 and Tables 6 and 7.

The calculations describe the O_2 binding by $[(H_3N)_3CuCu(NH_3)_3]^{2+}$ as an exothermic process with the R-state exhibiting a higher exothermicity than the T-state (by 2.2 kcal/mol; Figure 11). The calculated ΔH(s) values are larger than the experimentally determined values for O_2 binding of Hc proteins which lie in the range of −11.5 to −6.0 kcal/mol (Table 7).[72−76] This difference can be explained by the overly covalent bonding description of the oxy site on the B3LYP/Lanl2dz level (section 3.1.1). More quantitative agreement with experiment requires a more complete active site model and a density functional giving a better description of the copper-ligand bond.

The results for O_2 coordination by the mononuclear model complex show an exothermic process in which the peroxide complex $[\{(H_3N)_3Cu\}_2(\mu$-η^2:$\eta^2O_2)]^{2+}$ is 6.3 kcal/mol more stable than the isolated reactants and 6.9 kcal/mol more stable than an end-on bound superoxo intermediate $[(H_3N)_3$-

(67) The results of this Mulliken population analysis agree with NPA results.

(68) Analysis of the spin densities yields the same result.

(69) The metal−ligand bonding is inferred from the LUMO which has antibonding character. Analysis of the occupied orbitals is complicated by spin polarization.

(70) The electronic structure of the triplet state of a geometry with an $[Cu_2(\mu$-η^1:$\eta^2O_2)]$ core also exhibits orthogonal π^* orbitals.

(71) With the exception of the binuclear Cu(I) complex whose copper−copper distance has been kept fixed to the values indicated in Figure 11, all other minima are results of full geometry optimizations. The frequency calculations of the binuclear copper complexes exhibit very small imaginary frequencies (≥ -40 cm^{-1}). Although partial geometry optimization does not yield a true minimum on the energy surface, frequency calculations are used to estimate the zero-point corrections and other thermodynamic data.

(72) Antonini, E.; Brunori, M.; Colosimo, A.; Kuiper, H. A.; Zolla, L. *Biophys. Chem.* **1983**, *18*, 117−124.

(73) Er-El, Z.; Shaklai, N.; Daniel, E. *J. Mol. Biol.* **1972**, *64*, 341−352.

(74) Klarman, A.; Daniel, E. *Biochemistry* **1980**, *19*, 5176−5180.

(75) Zolla, L.; Kuiper, H. A.; Brunori, M.; Antonini, E. *Thermodynamics of Oxygen Binding to Helix pomatia β-Hemocyanin*; Marcel Dekker: New York, 1979.

(76) Brunori, M.; Kuiper, H. A.; Zolla, L. In *Life Chemistry Reports*; Wood, E. J., Ed.; Harwood Academic Publisher: New York, 1983; pp 239−250.

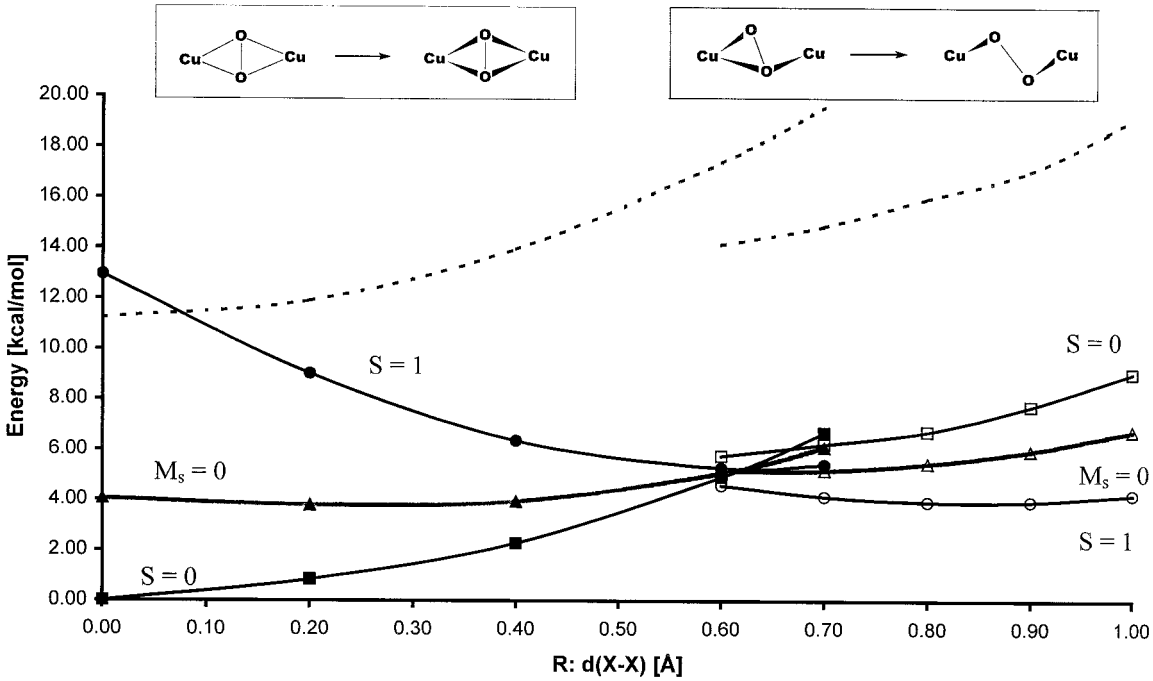

Figure 8. Potential energy surfaces of different spin states for the interconversion of oxyHc and deoxyHc: filled patterns, symmetric O_2 coordination, and hollow patterns, nonsymmetric O_2 coordination. The singlet state ($S = 0$) energy is spin-projected. To emphasize the importance of the broken-symmetry approach, results of the fully delocalized singlet state are included (dashed lines).

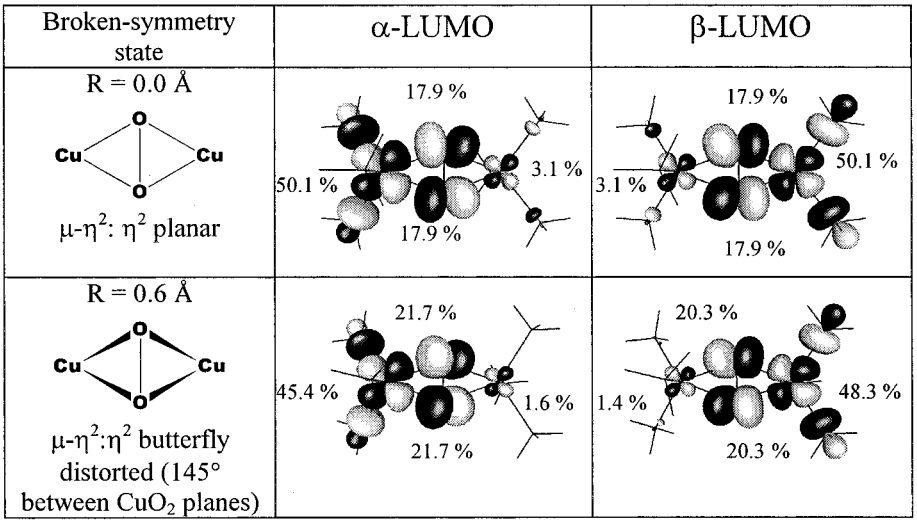

Figure 9. Surface plots of the α- and β-LUMO obtained from broken-symmetry calculations on stationary points with $R = 0.0$ and 0.6 Å. The Cu and O orbital contributions obtained from Mulliken Population Analysis are indicated.

Cu−O−O]$^+$.[77] In biomimetic model chemistry the O_2 reactivity of mononuclear complexes is increased by multidentate constrained ligands which enforce the copper(II) geometry on copper(I) complexes. This causes a destabilization of the copper(I) site relative to the cupric-peroxide complex. This is confirmed by a single-point calculation of the $[Cu(NH_3)_3]^+$ fragment with the geometry from the optimized side-on bound complex. This complex is around 15 kcal/mol less stable than the fully geometry optimized Cu(I) complex. Another study came to the same conclusion.[25]

The comparison of the calculated entropic changes (Table 7) during O_2 coordination for the binuclear Hc protein model system (R-state, −62.1 cal/(mol K); T-state, −58.7 cal/(mol K)) with that of the $[Cu(NH_3)_3]^+$ monomer (−77.8 cal/(mol K)) reflects the influence of the protein matrix in holding two copper(I) sites close together favoring O_2 binding. The calculated results for the Hc model are in reasonable agreement with the experimentally determined ΔS(s) in the reaction of binuclear biomimetic model complexes with O_2 (−46.85 and −39.44 cal/(mol K); Table 7).[13] However, the experimentally determined ΔS values of the proteins (−16.0 to −0.7 cal/(mol K); Table 7) are smaller than those of the binuclear model complexes which has been ascribed to contributions from the binding of allosteric effectors such as protons and calcium ions, to the allosteric transition, and to entropic changes in the protein structure.[72−76]

(77) It was also possible to find an η^2 bound superoxo complex that is slightly less stable than the end-on bound superoxo complex. However, frequency calculations do not characterize this geometry as a minimum. In comparison, an η^2 bound superoxo complex was experimentally characterized [Fujisawa, K.; Tanaka, M.; Moro-oka, Y.; Kitajima, N. *J. Am. Chem. Soc.* **1994**, *116*, 12079−12780]. The strained multidentate ligand in the latter likely contributes to its formation.

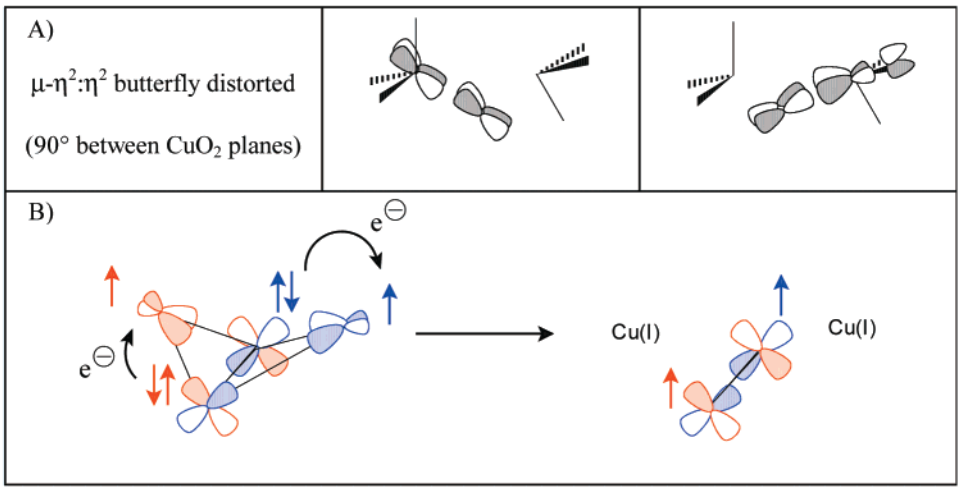

Figure 10. (A) Orthogonality of π^* O_2 orbitals eliminates charge contribution of second atom and therefore favors the ISC. (B) ET out of orthogonal π^* peroxide orbitals in the triplet state.

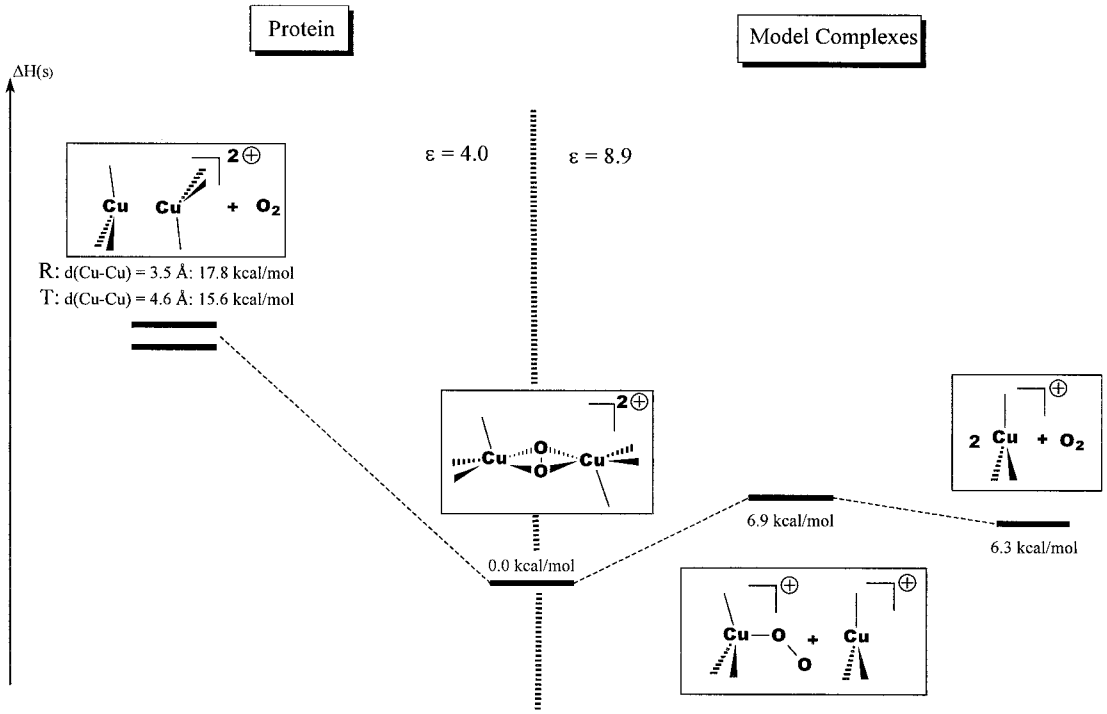

Figure 11. Energy minima of the binuclear (left: protein) and mononuclear model complexes (right) during different stages of the O_2 reduction. A mononuclear superoxo complex is included, which is not found for the binuclear models. The energy values are derived from spin projection, frequency, and PCM calculations. For clarity the NH_3 ligands are indicated by lines.

As a consequence of the differences in the calculated and experimentally determined ΔH(s) and ΔS(s) values between computational and experimental results for the Hc proteins, the ΔG(s) values differ in that the calculations exhibit a slightly endergonic reaction for the protein model systems (ΔG(s) values in Table 7), whereas experiments characterize the O_2 binding as a slightly exergonic process (protein: $\Delta G(s) = \sim -5.0$ kcal/mol; biomimetic model complexes: $\Delta G(s) = \sim -5.1$ to -4.4 kcal/mol). Also, the calculated energy difference between the relaxed and tense state ($\Delta\Delta G(s) = 1.15$ kcal/mol; Table 7) is smaller than the experimentally determined site−site interaction energy $\Delta\Delta G = \Delta G_{O_2}{}^{R} - \Delta G_{O_2}{}^{T}$ of 5.0 kcal/mol.[78] The inclusion of entropic effects strongly disfavors the binding of O_2 by the $[Cu(NH_3)_3]^+$ monomer fragment ($\Delta G(s) = +17$ kcal/mol, Table 7).

(78) Holm, R. H.; Kennepohl, P.; Solomon, E. I. *Chem. Rev.* **1996**, *96*, 2239−2314.

For mononuclear copper complexes the use of tailor-made multidentade ligands makes the O_2 process energetically feasible.[25] However, Hc accomplishes a favorable O_2 binding in a different way. As described in section 3.1.2, electrostatic repulsion destabilizes the $[(H_3N)_3CuCu(NH_3)_3]^{2+}$ site relative to isolated $[Cu(NH_3)_3]^+$ monomer complexes. As shown in Figure 11, this destabilization is a function of the copper−copper distance and remains after the inclusion of solvent effects. Thus, the protein holds the two Cu(I) ions in close proximity and the Cu(I) sites are destabilized relative to the binuclear side-on bound peroxide site, increasing the exothermicity of O_2 binding.

4. Discussion

This study continues our efforts to understand O_2 binding to Hc. Our past experimental data on oxy- and deoxyHc are used to calibrate DFT calculations which in turn are applied to study the reaction coordinate of O_2 binding. The O_2 release/binding

Table 6. Energies[a] for Optimized Geometries of Mono- and Binuclear Cu(I) and Cu(II) Complexes Optimized on the B3LYP/Lanl2dz Level (A PCM Model Has Been Applied for Solvents Calculations)

	state	E_{elec}(g)	ZPE	ΔH(g)[b]	ΔH(s)[b]	ΔG(s)[b]
$[Cu(NH_3)_3]^+$	^1A	−365.707340	0.116126	−365.581325	−365.647500[c]	−365.692704[c]
					−365.660175[d]	−365.705379[d]
O_2	$^3\Sigma_g^-$	−150.314740	0.003296	−150.308133	−150.308364[c]	−150.331736[c]
					−150.308434[d]	−150.331806[d]
$[(NH_3)_3Cu\text{-}O\text{-}O]^+$	^1A	−516.017079	0.121074	−515.881919	−515.967709[d]	−516.024657[d]
$[Cu_2(NH_3)_6]^{2+}$:						
d(Cu−Cu) = 3.5 Å	^1A	−731.322060	0.233130	−731.066185	−731.264276[c]	−731.347222[c]
d(Cu−Cu) = 4.6 Å		−731.331372	0.232857	−731.076505	−731.267745[c]	−731.349081[c]
$[\{(NH_3)_3Cu\}_2(\mu\text{-}\eta^2\text{:}\eta^2O_2)]^{2+}$ [e]	^1A	−881.670202	0.239627	−881.407808	−881.601021[c]	−881.677841[c]
					−881.638850[d]	−881.715670[d]

[a] In hartrees: 1 hartree = 27.2166 eV = 627.51 kcal/mol. [b] At 298 K; ΔH(s) and ΔG(s) are derived from corresponding values in the gas phase (ΔH(g) and ΔG(g)) corrected for the solvent contributions of $\Delta E_{elec} = E_{elec}(s) - E_{elec}(g)$. [c] $\epsilon = 4.0$. [d] $\epsilon = 8.93$. [e] Spin projected state.

Table 7. Comparison of Experimental and Calculated Data[a] of the O_2 Binding to Copper Complexes

	ΔH(s) [kcal/mol]	ΔS(s) [cal/(mol K)][b]	ΔG(s) [kcal/mol]
calculated data:			
$[Cu_2(NH_3)_6]^{2+} + O_2 \rightleftharpoons [\{(NH_3)_3Cu\}_2(\mu\text{-}\eta^2\text{:}\eta^2\ O_2)]^{2+}$			
R-state	−17.81	−62.11	+0.70
T-state	−15.63	−58.72	+1.86
$2\ [Cu(NH_3)_3]^{2+} + O_2 \rightleftharpoons [\{(NH_3)_3Cu\}_2(\mu\text{-}\eta^2\text{:}\eta^2\ O_2)]^{2+}$	−6.31	−77.82	+16.88
experimental data:			
deoxyHc + O_2 ⇌ oxyHc (protein)[c]	−11.5 to −6.0	−16.0 to −0.7	∼ −5.0
binuclear copper complexes[d]	−14.82, −13.86	−46.85, −39.44	−4.38, −5.06

[a] At 298 K, results from spin-projection. [b] $\Delta S(s) = (-\Delta G(s) + \Delta H(s))/T$. [c] Around room temperature from refs 72−76. [d] At 223 K from ref 13.

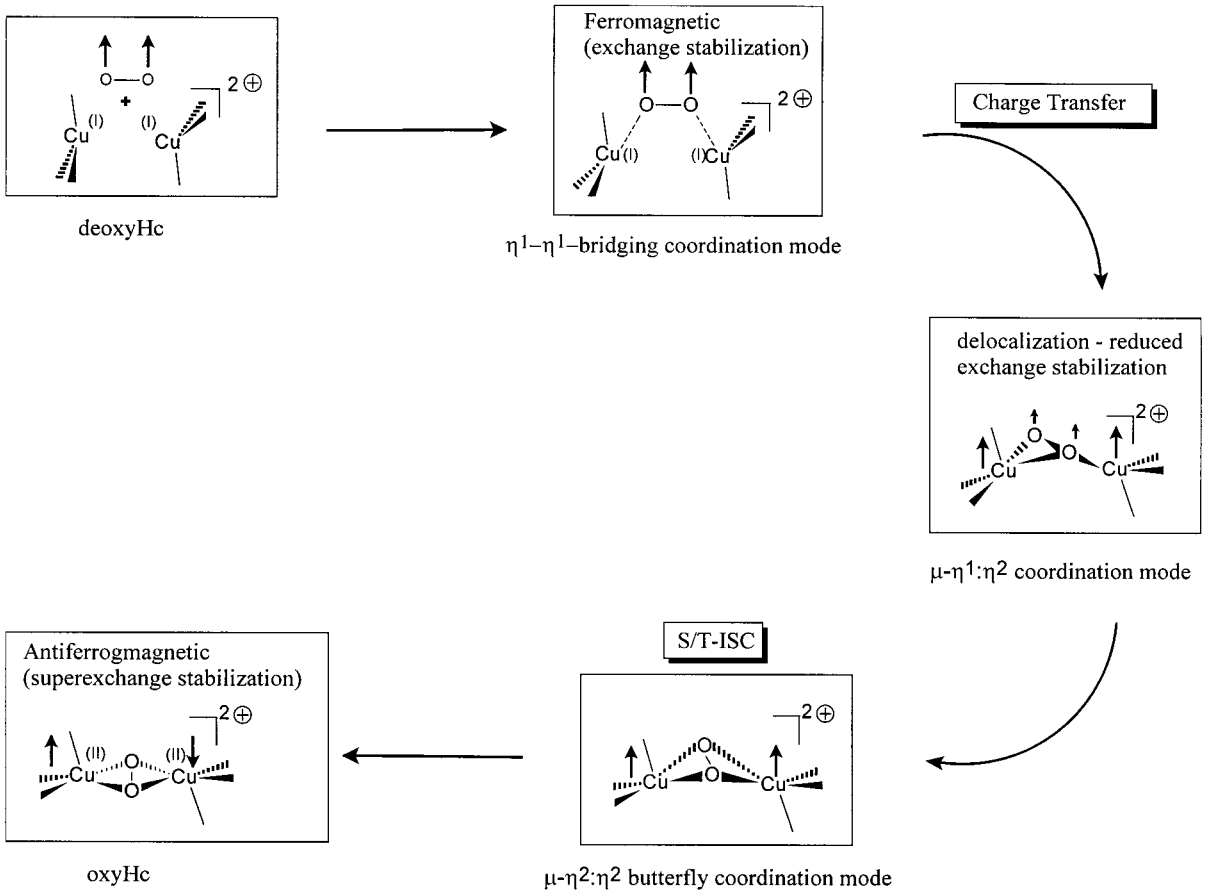

Figure 12. Schematic illustration of the relevant steps for O_2 binding to deoxyHc. The localization of unpaired electrons is indicated by arrows (up, α; down, β).

of Hc involves a two-electron-transfer process occurring at two metal centers. Therefore, the present study deals with whether a simultaneous or sequential ET takes place and how the spin-forbidden character of this process is overcome. Results for mononuclear model complexes are used to gain insight into the fundamental role of the protein in this reaction.

The method calibration reveals a qualitatively proper description of the electronic structure of the reactants and the side-on

bound peroxide complex which allows a discussion of the O_2 binding/release. This structure and reactivity correlation shows that the protein ligand reorientation upon O_2 binding destabilizes the redox active copper orbitals and thus favors the ET (Figure 5).

Figure 12 summarizes the mechanism developed here for O_2 binding to deoxyHc. O_2 approaches the binuclear copper(I) site driven to optimize the metal−ligand overlap. Calculations show that at early stages of O_2 binding when there is no significant interaction, pathways involving O_2 binding to one versus two coppers can compete. However, the closer O_2 approaches the binuclear copper site, the more the bridged binuclear binding mode is preferred. As the O_2 approaches, the coordination mode switches from end-on η^1-η^1-, to μ-η^1:η^2-, and then to μ-η^2:η^2-coordination, which derives from the increased bonding interaction between the substrate and the metal centers. This is in contrast to results of mechanistic investigations on biomimetic model systems.[13] For binuclear model compounds end-on superoxo intermediates are observed during O_2 binding. However, the preorganized binuclear copper site in the protein disfavors the formation of an end-on bound superoxo complex. The bridging interaction with both coppers enables the O_2 to be reduced by two electrons. This is consistent with the redox potentials[78] of O_2/O_2^- and O_2/H_2O_2 in aqueous solution ($E_{O_2/O_2^-} = -0.16$ eV vs $E_{O_2/H_2O_2} = +0.36$ eV) which favor two-electron chemistry and is supported by population analysis of the electronic structures for optimized geometries in their energetically lowest electronic configuration. A continuous CT from the two copper(I) centers into orthogonal oxygen-π^* orbitals occurs (Figure 7), indicating a simultaneous two-electron transfer.

At early stages of O_2 binding charge donation leads to the delocalization of the exchange stabilization onto the copper centers which are farer apart. This delocalization reduces the energy difference between the triplet and singlet state of the system. With increasing CT to the O_2, unpaired electrons evolve on the copper atoms which initially are ferromagnetically coupled due to close to orthogonal magnetic orbital pathways through the dioxygen ligand. The reduction of the butterfly distortion of the $Cu_2(\mu$-η^2:η^2 $O_2)$ core reduces the orthogonality of the magnetic orbitals and increases the superexchange coupling between the copper atoms which results in S−T ISC and then in a large stabilization of the singlet state (Figure 9) as observed by experiment.

Comparison with mononuclear model complexes indicates that the protein matrix holds the two copper(I) centers in close proximity, which enthalpically and entropically favors O_2 binding due to destabilization of the reduced binuclear site (Figure 11). This also allows regulation of the enthalpy by the change of the Cu−Cu distance in deoxyHc and provides an explanation for the origin of O_2 cooperativity in Hc proteins.

It is interesting to compare these results for Hc with the O_2 coordination pathway of Hr.[40] The active site of deoxyHr consists of a five- and six-coordinate iron in a binuclear iron(II) unit with a hydroxy and two η^1:η^1 carboxylate bridges. The remaining ligands are histidines. In OxyHr, O_2 binds as a hydroperoxide ligand to the originally five-coordinate iron(II) center and a binuclear iron(III) unit bridged by an oxo-ligand is formed. Thus, O_2 binding occurs at a single metal center and again involves a two-electron transfer, but in this case coupled to a proton transfer. As the triplet O_2 approaches along the open coordination site of the five-coordinate iron center of deoxyHr the increasing iron−dioxygen interaction decreases the pK_a of the bridging hydroxide and increases that of the O_2 ligand. A proton can be transferred to the O_2 species with concomitant single ET from the remote iron site via the formation of a σ/π oxo-superexchange pathway. During this proton-coupled electron transfer (PCET) ISC takes place whereby the proton transfer turns on the superexchange pathway. The formation of the μ-oxo diiron(III) site strengthens the antiferromagnetic coupling between the iron centers and thus the singlet state is strongly stabilized.

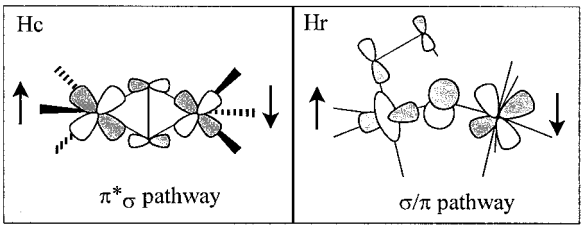

Figure 13. Lowest unoccupied α orbitals of the active site of oxyHc (left) and oxyHr (right). The contribution of the second metal ion to the spin orbital indicates the antiferromagnetic interaction of the occupied bonding counterparts.

There are some important differences and parallels between O_2 binding by Hc and Hr. The difference between both O_2 coordination strategies is the mechanism of CT. The reaction of O_2 with the two coppers held in close proximity by the protein matrix in Hc enables a simultaneous two-electron transfer, whereas O_2 coordination to one iron in Hr requires two sequential steps where one-electron transfer occurs from the remote iron center through the oxo-bridging ligand. Importantly a common theme emerges in these systems. The spin forbiddeness of the reactions is overcome by the CT from the two metal centers which shifts the spin density to the two metals and reduces the exchange stabilization of the $^3\Sigma_g^-$ ground state of O_2. The singlet state is further stabilized by coupling of the unpaired electrons on the metals through a superexchange pathway, either the peroxide bridge in Hc (the π^*_σ pathway) or the oxo-bridge in Hr (the σ/π pathway) (Figure 13). For both sites the superexchange pathway increases along the reaction coordinate for O_2 binding, either through flattening of the butterfly structure to produce the planar μ-η^2:η^2 structure in Hc or through the proton transfer to the peroxide ligand which forms the oxo-bridge in Hr.

In summary, this study has investigated the reaction coordinate of the reversible O_2 binding by Hc. The protein matrix holds two copper(I) centers in close proximity and therefore enables simultaneous 2-electron transfer. The exothermic character of the O_2 binding can be regulated by the Cu−Cu distance, which provides an explanation for the origin of O_2 cooperativity. Importantly the comparison with Hr reveals parallels in O_2 binding by binuclear metalloproteins. The spin forbiddeness of the reaction is overcome by delocalization of the exchange stabilization onto the two metal centers so that the energy difference between the triplet and the singlet state is small. In both cases, the superexchange pathways which form along the reaction coordinate enable the ISC and strong stabilization of the singlet state.

Acknowledgment. This work was partially supported by the National Computational Science Alliance under CHE990039N and utilized the NCSA SGI/CRAY Origin2000. Financial support for this research program came from NIH (DK-31450). M.M. thanks the Deutsche Akademische Austausch Dienst for a postdoctoral fellowship. The authors thank Dr. Robert K. Szilagyi for valuable discussions.

Supporting Information Available: The following data are included: S1, example of input file for broken-symmetry calculation in Gaussian 98; S.2, Cartesian coordinates of the optimized geometry of $[\{(NH_3)_3Cu\}_2(\mu\text{-}\eta^2\text{:}\eta^2O_2)]^{2+}$ in (A) the broken-symmetry state, (B) the closed shell singlet state, and (C) the triplet state; S3, Cartesian coordinates of the optimized geometry of $[(NH_3)_3Cu]_2^{2+}$ in the R-state and T-state; S4, optimized geometries describing the reaction coordinate of O_2 release/dissociation of the binuclear copper site in the T-state for (A) $R = 0.6$ Å (μ-η^2:η^2 coordination), (B) $R = 0.7$ Å (μ-η^1:η^2 coordination), (C) $R = 1.0$ Å (end-on η^1-η^1 coordination); S5, optimized geometries describing the reaction coordinate of O_2 dissociation from the binuclear copper site in the R-state for (A) $R = 1.4$ Å (μ-η^1:η^2 coordination), (B) $R = 1.6$ Å (end-on η^1-η^1 coordination), (C) $R = 2.0$ Å (end-on η^1-η^1 coordination), and (D) $R = 2.5$ Å (end-on η^1-η^1 coordination); S6, change of the partial charges and the spin densities during O_2 coordination to $[(NH_3)_3CuCu(NH_3)_3]^{2+}$ in the R-state; and S7, change of the partial charges and the spin densities during O_2 coordination to $[(NH_3)_3CuCu(NH_3)_3]^{2+}$ in the T-state (PDF). This material is available free of charge via the Internet at http://pubs.acs.org.

JA004166B